Lab on a Chip

PAPER

View Article Online
View Journal

Cite this: DOI: 10.1039/d5lc00060b

Lossless Altered Histone Modification Analysis System (LAHMAS)†

Zachary J. Kauffman, ‡[a] Kevin Koesser,‡[b] Kyle T. Helzer,[c] Marina N. Sharifi,[ad] Erika Heninger,[d] Chao Li,[d] Duane S. Juang,[b] David F. Jarrard,[e] Shuang G. Zhao,[cdf] Michael C. Haffner,[gh] David J. Beebe,§[bdi] Joshua M. Lang§[ad] and Jamie M. Sperger§*[ad]

Received 17th January 2025,
Accepted 18th June 2025

DOI: 10.1039/d5lc00060b

rsc.li/loc

Miniaturized biological assays using microfluidics have the potential to enhance assay sensitivity, reduce reagent consumption, and increase throughput. However, challenges to miniaturization include increased platform complexity and increased surface to volume ratios leading to risk of evaporation and analyte loss through surface binding. Exclusive Liquid Repellency (ELR) enables open microfluidic systems that minimize these challenges through an oil phase that protects small aqueous volumes from temperature fluctuation and evaporation while eliminating surface fouling that leads to sample loss. Here we report a novel microfluidic platform leveraging ELR and Exclusion-based Sample Preparation (ESP) for the miniaturization of CUT&Tag, a complex multistep biological assay. The resultant Lossless Altered Histone Modification Analysis System (LAHMAS) employs a PDMS–silane treated glass surface immersed in silicone oil to facilitate lossless liquid handling and prevent sample evaporation. The device design, compatible with standard laboratory equipment, allows effective processing of cell inputs as low as 100 cells with higher specificity than macroscale CUT&Tag facilitating accurate chromatin profiling of low input and rare cell samples.

Introduction

Epigenetic alterations, including histone modifications and DNA methylation, drive disease progression and treatment resistance in numerous pre-clinical models of cancer.[1–3] While identifying these alterations is possible using model systems, these analytes are more difficult to study in clinical settings. This is due to the fact that gold standard epigenetic profiling assays such as ChIP and CUT&Tag typically require tens to hundreds of thousands of cells in complex, multi-step assays.[4–7] Previous attempts to miniaturize epigenetic profiling, including analysis of chromatin structure,[8,9] DNA methylation,[10,11] or histone modification mapping,[12–20] have resulted in decreased input requirements and increased sequencing quality but ran into additional challenges. Multiple technologies leverage microfluidics for profiling low to ultralow input samples *via* miniaturized ChIP-based approaches by flowing chromatin fragments over packed[12] or fluidized[15] beds of antibody-coated beads, or through antibody-coated channels to eliminate the requirement for beads entirely,[14] though the complexity of these technologies may limit scalability. Additionally, tagmentation-based approaches, including CUT&Tag,[17] eliminate the need for crosslinking and shearing DNA. Such approaches improve efficiency, specificity of DNA recovery, and sensitivity for low input samples, but have not previously been miniaturized. We set out to manufacture a device with a generalizable design yielding a higher signal-to-noise ratio and specificity of sequencing from samples with less than 1000 cells.

The miniaturization of assays offers several possible advantages to overcome challenges inherent to macroscale assays including lower reagent consumption, higher throughput and lower waste. Yet, miniaturization often introduces new challenges, since low liquid volumes are prone to temperature fluctuation, evaporation, mishandling, and sample loss during

[a] Department of Medicine, University of Wisconsin–Madison, Madison, WI, USA. E-mail: jsperger@medicine.wisc.edu
[b] Department of Biomedical Engineering, University of Wisconsin–Madison, Madison, WI, USA
[c] Department of Human Oncology, University of Wisconsin–Madison, Madison, WI, USA
[d] Carbone Cancer Center, University of Wisconsin–Madison, Madison, WI, USA
[e] Department of Urology, University of Wisconsin–Madison, Madison, WI, USA
[f] William S. Middleton Memorial Veterans Hospital, Madison, Madison, WI, USA
[g] Divisions of Human Biology and Clinical Research, Fred Hutchinson Cancer Center, Seattle, Washington, USA
[h] Department of Laboratory Medicine and Pathology, University of Washington, Seattle, Washington, USA
[i] Department of Pathology and Laboratory Medicine, Madison, WI, USA

† Electronic supplementary information (ESI) available. See DOI: https://doi.org/10.1039/d5lc00060b

‡ ZJK and KK contributed equally.

§ DJB, JML and JMS jointly supervised.

processing.[21–23] Fouling, the undesired adsorption of molecules onto a solid surface, is a key mechanism by which biological analytes can be lost, and is exacerbated by the increased surface area to volume ratio at the microscale.[24]

Exclusive Liquid Repellency (ELR) enables under-oil open microfluidic systems (UOMSs) that seize the advantages of miniaturization while mitigating the challenges.[21,25,26] ELR is an inherent phenomenon in which an aqueous droplet can be fully repelled from a solid surface (Young's contact angle = 180°) in the presence of an immiscible oil phase when the sum of the interfacial energies of the solid/oil and aqueous/oil interfaces is less than or equal to the solid/aqueous interfacial energy.[27] We have previously demonstrated that these conditions can be met by employing a polydimethylsiloxane (PDMS)–silane functionalized surface paired with silicone oil as the oil phase.[21] Open microfluidic methodologies have been developed with antifouling properties, such as coating aqueous entities with hydrophobic particles to create liquid marbles and liquid plasticines, with spherical and complex shapes, respectively.[28–31] These techniques achieve antifouling effects similar to those of ELR by employing a thin layer of hydrophobic particles instead of oil. Unlike ELR, these techniques allow the manipulation of discrete droplets in air. However, ELR is particularly advantageous for small volume bioassays requiring high temperature incubation, since the oil phase reduces evaporation.[21] While other systems have employed an oil phase to protect small aqueous volumes from temperature fluctuation and evaporation, ELR simultaneously eliminates surface fouling, which reduces the loss of samples to adsorption on the substrate.[21,23,27,32]

Using ELR-enabled UOMSs to perform epigenetic analysis requires integration with methods for capture and extraction of analytes. Exclusion-based Sample Preparation (ESP) is a validated method for the capture and extraction of rare or low abundant analytes. ESP refers to a collection of solid-phase analyte extraction techniques by which analytes bound to a solid-phase (magnetic beads) can be extracted out of a complex sample by transporting the beads *via* a magnet through an immiscible interface (oil or air) to "exclude" non-target contaminants from the sample.[33–40] The ESP process replaces the multiple washing operations in traditional solid-phase extraction techniques with a simple magnetic dragging operation through immiscible interfaces, resulting in a much shorter processing time and higher sample recovery. Recently, we have developed lossless processing methods applying PDMS–silane/silicone oil-based ELR for SARS-CoV-2 detection (OIL-TAS)[22] and applying magnetic bead-based ESP for methylated DNA enrichment (SEEMLIS).[41] Using a similar device described herein, we demonstrate that complex biological assays can be improved *via* miniaturization.

We used the ESP and ELR-based microfluidic systems to miniaturize the Cleavage Under Targets and Tagmentation (CUT&Tag) assay and termed it the "Lossless Altered Histone Modification Analysis System" (LAHMAS). CUT&Tag was developed as an alternative to chromatin immunoprecipitation (ChIP) to investigate protein–DNA interactions with high resolution, lower background, and decreased cellular input requirements than traditional ChIP.[17] CUT&Tag has been used to assess histone modification in numerous settings including the central nervous system, mixed-lineage leukemias, and prostate cancer organoids.[42–44] In contrast to traditional ChIP, CUT&Tag performs well in samples with as few as 10 000–50 000 cells and has been successfully performed with as few as 60 cells.[17] However, performance is less reliable for inputs below 5000 cells, making analysis of rare cell samples such as tumor biopsies and circulating tumor cells difficult. Therefore, we aimed to adapt the CUT&Tag assay for use on a microfluidic device to mitigate analyte loss associated with this complex, multi-step epigenetic assay and facilitate routine analysis of low input (<1000 cells) clinical samples such as prostate cancer organoids derived from primary tissues such as those from prostatectomy. CUT&Tag utilizes a paramagnetic particle based approach to compartmentalize nuclei for isolation and library preparation of the protein-bound DNA of interest.[4,17,45] Here we utilized the same paramagnetic particle based nuclear compartmentalization in conjunction with our microfluidic ELR/ESP platform to miniaturize the entire multi-step CUT&Tag assay on the device. We show that performing CUT&Tag on the LAHMAS device increases the signal to noise ratio in the peak, calling for very low input samples, which enables the investigation of chromatin dynamics in rare cell sample types, including patient derived organoids, biopsies, and circulating tumor cells.

Experimental

Preparation of polycarbonate inserts and chamber slides

Polycarbonate inserts were milled from 4 mm sheets (TAP Plastic). Inserts were deburred and rinsed with isopropanol (IPA) then sonicated in IPA for 1 hour using a bench-top ultrasonic cleaner (Branson 2510). The inserts were dried in an oven at 60 °C for 1 hour. To silanize, the inserts were treated with O_2 plasma (Diener Femto) at 100 W for 3 minutes (flow: 5 sccm). 10 μL of deionized water was then pipetted on the inserts and observed with a goniometer (Rame-Hart Model 200). Fabrication only proceeded if the observed contact angle was below 30 degrees. The inserts were then placed in a 60 °C oven for 3 hours with 100 μL 1,3-dichloro-1,1,3,3-tetramethyldisiloxane (Gelest). The inserts were sonicated in IPA for 1 hour. Polycarbonate chamber slides were milled from 4 mm sheets (TAP Plastic). Side pieces were deburred and rinsed with IPA prior to sonication in IPA for 1 hour. Dry side pieces were fused together with acetonitrile to form a chamber prior to drying at 60 °C for 10 minutes. Sides were rinsed with IPA and dried in an oven at 60 °C for 1 hour.

Preparing glass bottom and assembling the chambers

#1.5 borosilicate glass slides (Fisherbrand, Corning) were silanized as described above. The center of each treated slide was masked with Scotch tape (3M) and treated with O_2 plasma (Diener Femto) at 100 W for 1 minute to etch the

silanized surface from slide edges. Gorilla Glue super glue was applied sparingly to the bottom of assembled polycarbonate chamber sides and bonded to the etched glass slides. Assembled devices were placed in an oven at 60 °C with a small tray of DI water for 1 hour to cure. Devices were rinsed with IPA.

Fouling test

Adsorption-based fouling was utilized to test the ELR treatment in the devices after fabrication. Cell culture media containing 10% FBS and 1 μM fluorescein were added to the devices for overnight incubation. The devices were then inverted to drain the liquid and imaged under ultraviolet light to determine the extent of adsorption-based fouling (Fig. S1†). Any presence of fluorescein after the devices were drained of the liquid constituted a failure, since ELR must be ubiquitous across every surface to completely repel aqueous reagents. Unfouled devices were rinsed thoroughly with IPA before use.

Buffer preparation

Nuclear extraction (NE) buffer was made with 20 mM HEPES-KOH pH 7.9, 10 mM KCl, 0.1% Triton X-100, 0.5 mM spermidine (Cell Signaling Technology 27287), 1 : 200 protease inhibitor cocktail (200×, PIC) (Cell Signaling Technology 7012), and 20% glycerol. Wash 150 buffer was made with 1× wash buffer (Cell Signaling Technology 31415), 0.5 mM spermidine, and 1× PIC. Wash 300 buffer was made with wash 150 buffer and 150 mM NaCl. Dig-150 buffer was made with wash 150 buffer and 0.05% digitonin. Dig-300 buffer was made with wash 300 buffer and 0.05% digitonin. Tagmentation buffer was made with Dig-300 buffer and 10 mM $MgCl_2$ (Thermo Scientific R0971). HALT buffer was made with 10 mM TAPS (Boston BioProducts BB-2375) and 1.2 mM EDTA. TAPS buffer was made with 10 mM TAPS and 0.2 mM EDTA. SDS release buffer was made with 10 mM TAPS and 0.1% SDS (Active Motif 53176).

ConA bead preparation

10 μL of concanavalin A (ConA) beads per sample were resuspended in 100 μL per sample of cold bead activation buffer (Cell Signaling Technology 93569S). The beads were washed twice then resuspended in 10 μL per sample bead activation buffer. The beads were aliquoted into 10 μL of activated bead slurry per sample.

Cell culture

LNCaPs were from ATCC and passaged utilizing 0.25% trypsin (Cytiva SV3003101) and RPMI media (Corning MT10040CV). Cells were maintained at 37 °C and 5% CO_2 in an RPMI culture medium supplemented with 10% fetal bovine serum (R&D Systems S11550H), 2% penicillin (Gibco, 15140-122), and 1% HEPES (Corning 25-060-CI).

Nuclei preparation and binding nuclei to activated beads

LNCaP cells in a T75 flask were washed with 2–5 mL phosphate buffered saline (PBS, Gibco 10010072) and trypsinized with 0.05% trypsin (Cytiva SH30236.01). 500 000 cells were aliquoted for the CUT&Tag assay. Cells were resuspended in 500 μL cold 1× NE buffer and incubated for 10 minutes on ice. An indicated number of nuclei was added in 100 μL aliquots. 10 μL activated ConA beads were added to each 8-strip tube, vortexed to mix and incubated for 10 minutes at RT to bind.

Patient derived cancer organoids

Human prostate cancer tissue was obtained at the University of Wisconsin–Madison from patients undergoing radical prostatectomy who had received no prior treatments. The study was conducted in compliance with the Guidelines and Declaration of Helsinki. The University of Wisconsin Institutional Review Board has approved the utilization of all the tissue samples in this study (IRB# 2017-0878) and written and informed consents have been obtained from all patients. Prostate tumor tissue was sampled by gross dissection from surgical prostatectomy specimens at the TSB Biobank at the University of Wisconsin Carbone Cancer Center. Organoids used for this study were generated as previously described.[46] Briefly, enzymatically digested prostate tissue isolates were seeded in 50% growth factor reduced-Matrigel™ (BD Biosciences, CA) in hanging droplets in a 24-well plate (Greiner). The plate was inverted then placed into a cell culture incubator at 37 °C and 5% CO_2 for 40 min to solidify the droplets prior to feeding with 1 mL PrEGM media (Lonza) supplemented with 10 uM Y-27632 (Sigma-Aldrich, MO). Organoids were digested down to single-cell resuspension with 1 mg mL^{-1} collagenase at 37 °C and 5% CO_2 for 10 min. Cells were resuspended in 500 μL cold NE buffer and incubated for 10 minutes on ice. 10 μL activated ConA beads were added, vortexed to mix and incubated for 10 minutes at RT to bind.

Antibody binding to chromatin proteins

ConA bound nuclei were resuspended in 15 μL of normal rabbit IgG polyclonal primary antibody (Cell Signaling Technology 2729) or Tri-Methyl-Histone H3 (Lys27) (C36B11) rabbit monoclonal primary antibody (Cell Signaling Technology 9733) diluted 1 : 50 in Dig-150 buffer per sample. The nuclei suspension was added into the first well of the device and resuspended with an oil-primed pipette. These samples were incubated shaking on an orbital shaker plate overnight at 4 °C. 15 μL of goat anti-rabbit IgG secondary antibody (EpiCypher 13-0047) diluted 1 : 100 in Dig-150 buffer was pipetted into well 2 of each device. A bead bolus was resuspended in well 1 until homogeneous with an oiled pipette. A magnet was used to drag beads from well 1 to well 2. Samples were resuspended with an oiled pipette until homogeneous. Each device was placed on an orbital shaker plate at RT for 60 minutes. The samples were taken off the

shaker to add 17.5 μL cold digitonin 150 (Cell Signaling Technology 16359L) buffer to wells 3 & 4. The magnet was used to drag the bead bolus into well 3 followed by resuspension with an oil-primed pipette until homogeneous. This process was repeated in well 4.

Binding pA-Tn5 transposase

15 μL of 1× CUTANA pAG-Tn5 (EpiCypher 15-1017) diluted 1 : 20 in Dig-300 buffer was added to well 5. A bead bolus was dragged to well 5 using a magnet and resuspended with an oiled pipette until homogeneous. Samples were incubated on an orbital shaker plate at RT for 60 minutes. 17.5 μL digitonin 300 buffer was added directly to wells 6 & 7. The bead bolus was dragged to well 6 using a magnet and resuspended until homogeneous. This process was repeated in well 7.

Targeted chromatin tagmentation

The device was removed from the magnet and 15.0 μL tagmentation buffer was added to well 8. A bead bolus was dragged to well 8 using a magnet. The sample was resuspended with an oiled pipette until homogeneous then incubated for 55 minutes at 37 °C in an oven. 2.5 μL HALT buffer was added to the sample in well 8 to quench the remaining active Tn5 prior to transfer. 17.5 μL TAPS buffer was added to well 9 to wash out unbound Tn5. The bead bolus was dragged to well 9 and resuspended with an oiled pipette until homogeneous.

DNA extraction

5 μL RT 0.1% SDS release buffer was added to well 10. A bead bolus was dragged to well 10 with a magnet and incubated for 55 minutes at 58 °C. 15 μL RT SDS quench buffer (0.67% Triton-X, Thermo Scientific Chemicals 327371000) was then added to well 10. An oil-primed pipette was used to move samples to tubes before they were vortexed prior to PCR amplification.

Library amplification

4 μL of Illumina indexed primers (10 μM stocks, Illumina 20027213) and 25 μL CUTANA non-hot start 2× Master Mix for CUT&Tag (EpiCypher 15-1018) was added to the sample and mixed. The PCR protocol [hold at 58 °C, 5 minutes at 58 °C; 5 minutes at 72 °C; 45 seconds at 98 °C; 15 seconds at 98 °C; 10 seconds at 60 °C; 13 cycles of (15 s at 98 °C & 10 s at 60 °C; 1 minute at 72 °C) hold at 4 °C] was performed to amplify the DNA.

Library clean-up

DNA cleanup of samples was performed using 1.3× AMPure beads (Beckman Coulter A63881). The sample was incubated for 5 minutes at RT prior to magnet binding and supernatant removal. The sample was then washed twice with freshly made 200 μL 80% EtOH (Fisher BioReagents BP2818500) with 1 minute incubation. The samples were dried up to 3 minutes. DNA was eluted from the sample in 15 μL EB buffer (Qiagen 19086). The library DNA concentration was measured using a 1× Qubit dsDNA HS (High Sensitivity) Assay kit (Thermo Scientific Q33231) and the library size was quantified from 2 μL of sample using the TapeStation High sensitivity D1000 ScreenTape and reagents (Agilent 5067-5584 and 5067-5585).

Bioinformatic pipeline

The samples were sequenced at the University of Wisconsin–Madison Biotechnology Center's DNA Sequencing Facility (Research Resource Identifier – RRID:SCR_017759) for paired end sequencing (2 × 150) with a target depth of 10 million reads. Sequencing data were aligned to human hg38 genome with BWA-mem.[47] Aligned reads were combined by shared replicate assays and significant peaks were called with PePr[48] using a *p*-value threshold of 0.01. IgG reads were used as a background in every separate condition for H3K27Me3 peak calling. To define a broad range of H3K27Me3 occupancy regions among the LNCaP samples in a similar fashion to low-input CUT&Tag,[17] a union peak set was formed from all called H3K27Me3 peaks among a previously unpublished large-scale (>10 000 cells per sample) LNCaP CUT&Tag dataset. The fraction of reads that fell in peaks (FRiP) of this union peak set, the major quality control metric representing a measure of the signal-to-noise ratio adopted by the ENCODE project,[49] was calculated from all unique fragments from sequencing reads of a sample falling within the union peak set. We generated FRiP scores after peak calling on a sample-by-sample basis. For peak calling utilizing the patient derived organoid sample, we performed peak calling and calculated FRiP utilizing MACS2,[50,51] as a union peak set was not available. The bioinformatic workflow is shown in Fig. S2.† Bed files were stored at doi: **https://figshare.com/s/9b1a81f49ed98c0b5a7b**.

Results & discussion

LAHMAS device design

Depicted in Fig. 1, the LAHMAS device includes a silicone oil-filled glass-bottom chamber with a removable milled polycarbonate well insert. All solid surfaces are covalently modified with PDMS–silane to establish ELR and prevent adsorption-based sample loss. As illustrated in Fig. 1A(i), the contact angle between the aqueous phase and the solid substrate is 180 degrees in the silicone oil. The polycarbonate insert includes 10 discrete holes connected by a single continuous channel through which paramagnetic particles – but not aqueous droplets – can pass, thereby creating independent reaction wells for each step of the CUT&Tag procedure with no crosstalk. This design employs Exclusion-based Sample Preparation (ESP), which refers to a collection of solid-phase analyte extraction techniques by which analytes bound to a solid-phase (magnetic beads) can be extracted out of a complex sample by transporting the beads

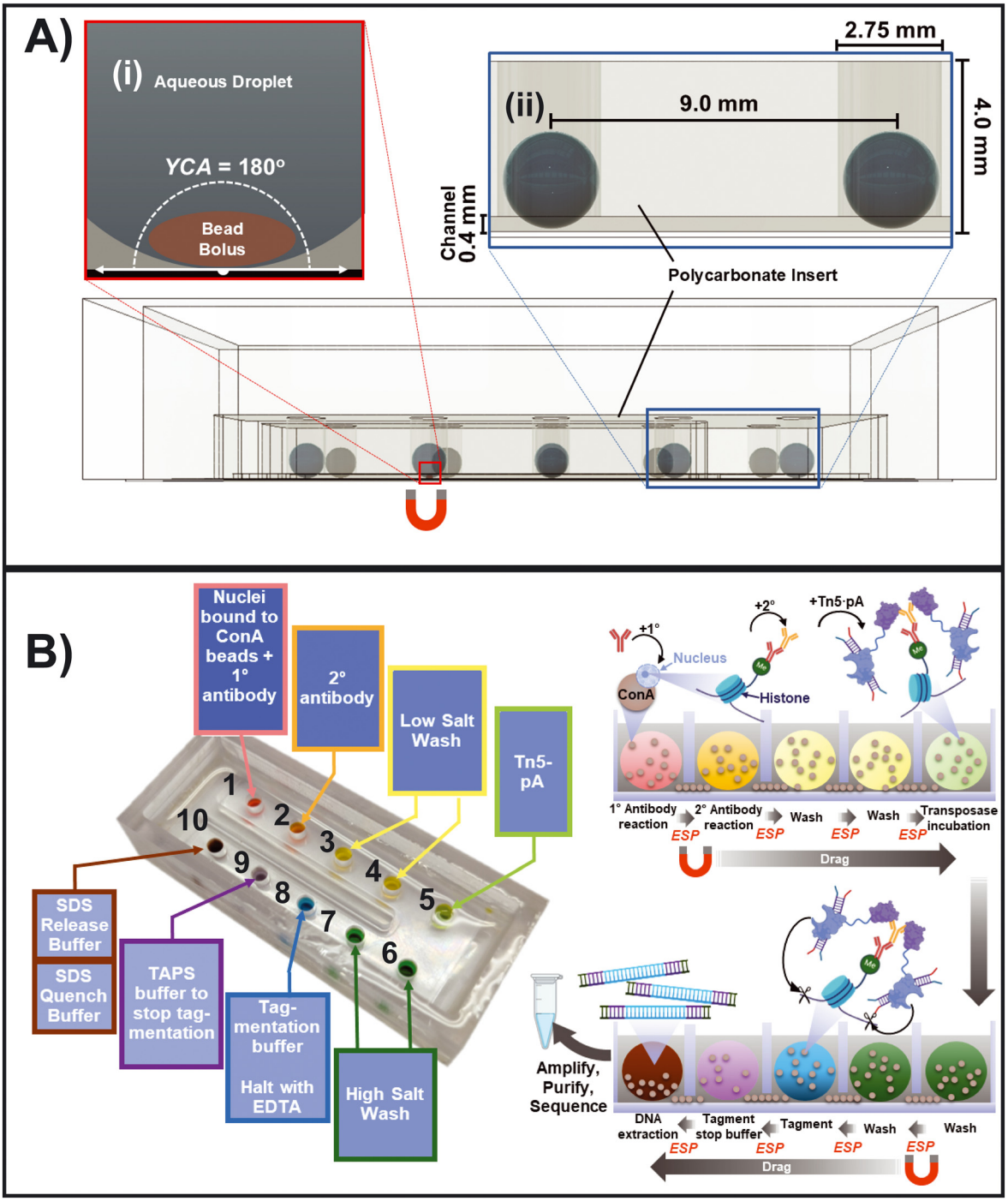

Fig. 1 A) Schematic depicting the dimensions of the reagent wells and the 0.4 mm channel (ii) through which magnetic beads pass. Young's contact angle in each reagent droplet remains 180 degrees due to ELR, which limits adsorption-related sample loss. (i) ESP is used to gently transfer magnetic beads to each reaction well with minimal carryover volume. B) Image and schematic depicting the design and biochemical steps performed for CUT&Tag reactions on the LAHMAS device.

via a magnet through an immiscible interface (inert oil) to exclude non-target assay reagents from the sample, resulting in shorter, gentler processing and higher sample recovery. The oil phase fully separates the individual droplets in the device, as the hydrophilic and amphiphilic aqueous reagents do not diffuse into the oil phase.[21] The hydrophilic nuclei and beads, when magnetically pulled between aqueous droplets through the oil phase, maintain a thin layer of aqueous fluid separating the analyte from the oil. The silicone oil overlay minimizes evaporation and external contamination from aerosols in the microliter-scale reagents. Likewise, polycarbonate and glass are resilient to heating and cooling necessary during the CUT&Tag assay (between 4 °C and 58 °C), enabling antibody binding, enzymatic reactions,

and DNA elution to be performed *in situ*. The clear, 150-micron glass bottom minimizes the distance between magnetic beads in the device and the magnet outside the device and facilitates imaging on light or fluorescence microscopes. Furthermore, the device geometry features the same 9 mm well pitch as a conventional multi-well plate, enabling liquid handling *via* multi-channel pipettes and data acquisition with plate readers or microscopes (Fig. 1A(ii)). Additionally, this device has 24 μL wells and 400 μm tall channels to permit a range of reagent and bead volumes between 4 and 24 microliters. The modular design allows the component parts to be treated and cleaned easily, improving surface uniformity and possibly enabling the cleaning and reuse of devices, pending further validation. Moreover, while the inserts were designed for low cell inputs, inserts with larger well diameters and channel height could be fabricated and used with the same chambers if higher cell inputs are required.

The LAHMAS platform contains 10 discrete droplets to perform the CUT&Tag procedure (Fig. 1B). Each step of the method occurs in a discrete well, numbered 1–10 in Fig. 1B. Primary antibody binding occurs in well #1, followed by secondary antibody binding in well #2, two washes (wells 3 and 4), transposase binding (well 5), two high salt washes (wells 6 and 7), transposase activation and halt (well 8), TAPS wash (well 9), and cell lysis and quench (well 10). Movie S1† demonstrates how beads are magnetically moved between the wells. Each wash step uses two wells to mitigate any possible effects of carryover between adjacent wells *via* the thin layer of aqueous liquid that surrounds the beads and nuclei. Library amplification is performed off device using standard procedures.

LAHMAS oil viscosity optimization

Efficient movement of the bead bolus from one droplet to the next is essential to minimize the loss of nuclei (and therefore DNA) in this assay. Several forces act on the bead–droplet system when manipulating magnetic beads (Fig. 2A). While the magnetic force acts to clump the beads together and separate the beads from the droplet, capillary force and viscous forces resist the consolidation of the beads and the deformation of the droplet. The Ohnesorge number, $\left(\mathrm{Oh} = \frac{\mu}{\sqrt{\rho\sigma L}}\right)$, compares the relative contribution of viscous forces *versus* that of inertia and interfacial tension. At higher Ohnesorge numbers, inserted energy is converted into internal viscous dissipation.[52] In our system, that means the force of the magnet deforming the droplet is dissipated. While this effect is desired to prevent the droplet from deforming so much that multiple wells combine, too much viscous force dissipation will prevent the magnetic bead

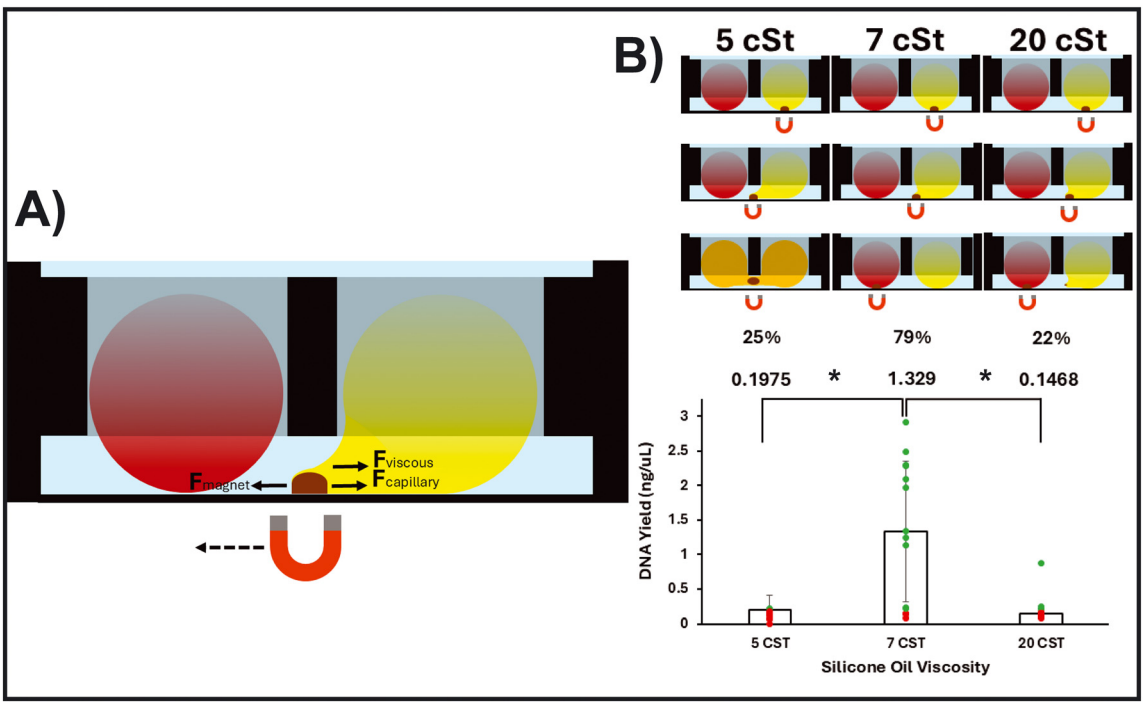

Fig. 2 A) A uniaxial representation of forces at play during magnetic bead translation. B) Top: A schematic depicts a side view of the device during magnetic manipulation using silicone oil of different kinematic viscosities. 5 centistoke (cSt) silicone oil is thin enough to permit significant deformation of the reagent droplets, occasionally combining discrete reaction wells. 20 cSt silicone oil is thick enough to prevent deformation of the reagent droplets, occasionally overcoming the force of the magnet and leaving some analyte behind while moving the beads from one well to another. 7 cSt silicone oil allowed optimal deformation of the droplets to move the beads from one well to another. Bottom: The DNA yields using different kinematic viscosities of silicone oil (*$p < 0.0001$). The success rate and yields denoted are from a side-by-side comparison of the three oil types while the schematic depicts the observed flaws encountered under the 5 cSt and 20 cSt conditions.

bolus from breaking off from the droplet and transferring efficiently to the next droplet. Consequently, the viscosity of the silicone oil bathing the device has a significant impact on bead bolus transfer. To optimize bead bolus transfer, we evaluated the performance of 5, 7, and 20 centistoke (cSt) silicone oil for CUT&Tag with a 1000 cell input. We observed that 7 cSt silicone oil allowed optimal deformation of the droplets to move beads from one well to another. In a side-by-side comparison, we also observed that using 7 cSt silicone oil resulted in significantly increased DNA yield (1.329 ng μL^{-1}) compared to 5 cSt (0.1975 ng μL^{-1}, $p < 0.0001$) and 20 cSt (0.1468 ng μL^{-1}, $p < 0.0001$) (Fig. 2B).

DNA yield and sequencing quality metrics

To test the efficiency of the CUT&Tag assay in the LAHMAS device with low input samples, we utilized the LNCaP prostate cancer cell line across a range of nuclei inputs, using an anti-Histone H3 lysine 27 trimethylation (H3K27Me3) antibody as this is an abundant histone modification in LNCaP cells.[4,53] We compared assay metrics from the microscale procedure done in the LAHMAS device (micro) to the standard macroscale procedure done in standard 0.2 mL PCR tubes (macro). We observed that the samples processed using the micro procedure had a significantly lower average yield than using the macro procedure with inputs between 1000 and 5000 nuclei (3.475 ng μL^{-1} *vs.* 7.419 ng μL^{-1}, $p = 0.0033$) (Fig. 3A). However, when we decreased the cell input to <1000 nuclei, the yields were not significantly different (1.009 ng μL^{-1} *vs.* 1.048 ng μL^{-1}, $p = 0.8984$) (Fig. 3B). This narrowing gap in yields as the input is decreased is displayed by the significantly different converging slopes ($p = 0.0034$) of microscale and macroscale $\log_2$DNA yields (Fig. 3C).

To assess the quality of the libraries after sequencing, we measured the sequencing depth, percent of reads aligned, number of unique reads and fraction of reads in peaks (FRiP). The sequencing depth, percent of reads aligned, and number of unique reads are common metrics used to assess the quality of all next generation sequencing. CUT&Tag can generate high quality data with as few as 2–5 million reads. All samples surpassed 3 million reads (Fig. S3A†). The percent of reads aligned should be >80% for high quality sequencing including CUT&Tag. All but 3 samples surpassed this threshold (Fig. S3B†). The unique reads are affected by the cell number as the starting concentration DNA (as well as the total copies of each gene) is limited by the total cell input. As expected, unique reads were lower in very low input samples (<1000 nuclei) compared to higher input samples (1000–5000 nuclei) (Fig. S3C†). Despite unique reads being higher in the macroscale compared to the microscale for the higher input samples (1000–5000 nuclei), the unique reads were similar between the microscale and macroscale at the very low input samples (<1000 nuclei), similar to what we observed with the total DNA yield (Fig. 3A and B).

FRiP is a quality control metric used in ChIP, CUT&Tag and assay for transposase-accessible chromatin (ATAC) sequencing

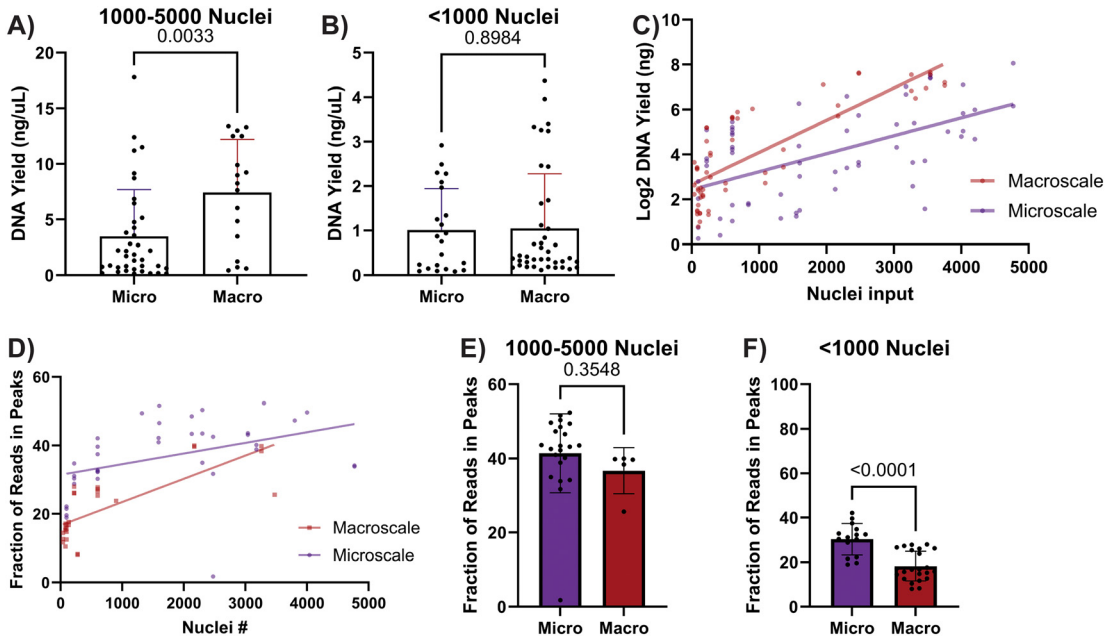

Fig. 3 DNA yield (purple, micro; red, macro) for H3K27Me3-tagged CUT&Tag assays performed in A) with 1000–5000 nuclei (microscale ($N = 38$) and macroscale ($N = 17$)) or B) with inputs less than 1000 nuclei (microscale ($N = 22$) and macroscale ($N = 40$)). C) Yield of CUT&Tag samples prepared in the microscale ($N = 60$) and macroscale ($N = 57$) *versus* number of nuclei input. D) FRiP scores of CUT&Tag samples prepared in microscale ($N = 39$) and macroscale ($N = 28$) devices *versus* number of nuclei input. Fraction of reads in peaks (FriP) of H3K27Me3-tagged CUT&Tag assays performed with E) nuclei inputs between 1000 and 5000 (microscale (purple, $N = 24$) and macroscale (red, $N = 5$)) or F) and nuclei inputs less than 1000 nuclei (microscale (purple, $N = 15$) and macroscale (red, $N = 23$)).

data to assess the signal-to-noise ratio, with higher values indicating a greater signal-to-noise ratio in the data. For ChIP assays, a FRiP of 1% is generally considered adequate[49] whereas one of the advantages of CUT&Tag is that FRiP scores are generally higher, achieving 34% and 58% of pooled single cell-H3K27Me3 reads in K562 and H1 cells, respectively.[17] Notably, standard peak-calling approaches are not optimized for use with low input samples with lower numbers of unique reads. That study instead defined FRiP scores as the percentage of the signal in the regions where peaks are located in a union peak set of sequencing in bulk samples. We have incorporated a similar method in this manuscript. Here we observed passing

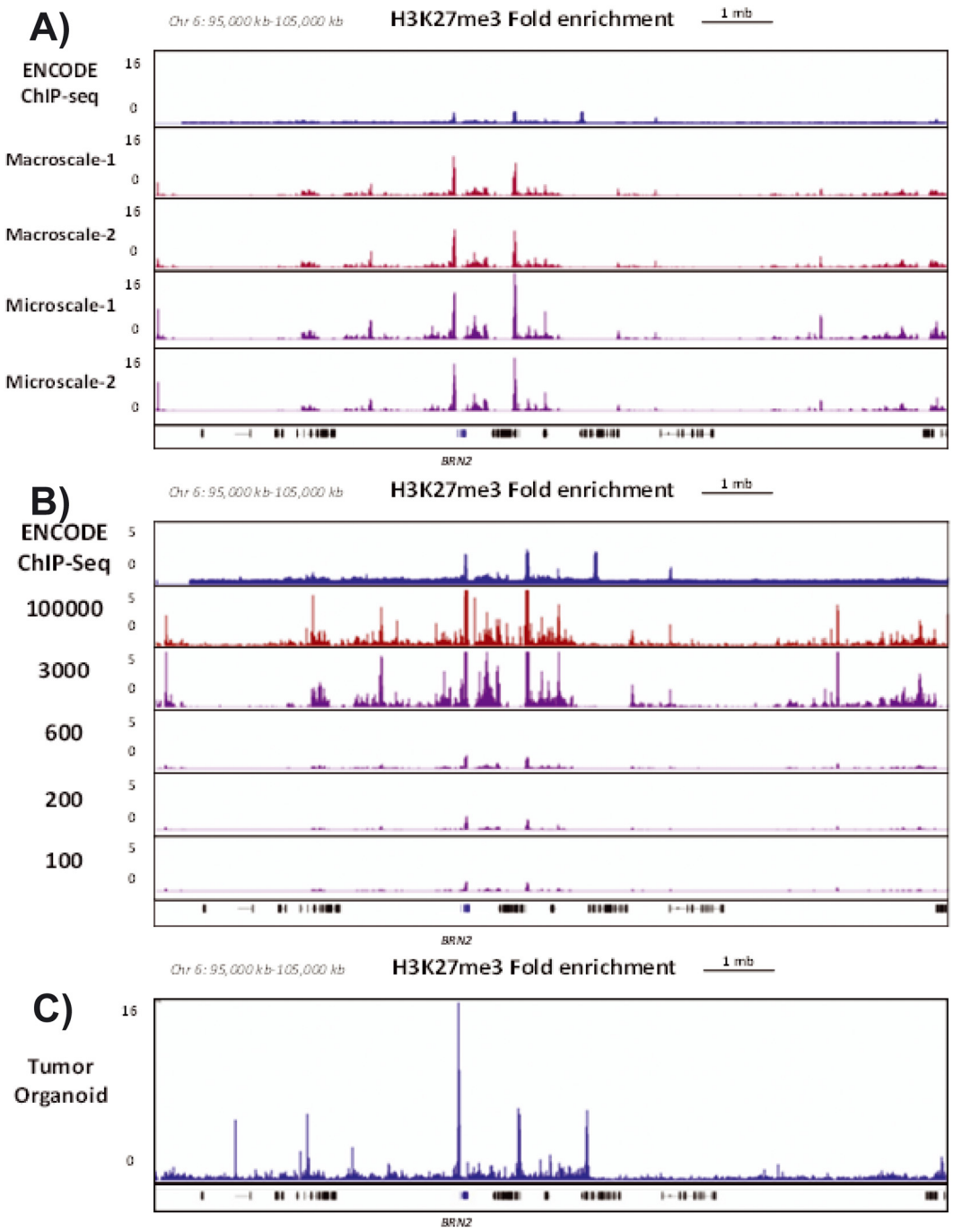

Fig. 4 Genome browser profiles of H3K27Me3-tagged DNA fold enrichment over IgG control visualized on IGV viewer chromosome 6 from 95 000–105 000 kb. CUT&Tag assays were performed with A) 3000 LNCaP nuclei in duplicate on the macroscale and microscale compared to publicly available LNCaP ChIP-seq ("ENCODE ChIP-Seq"), B) titration of 3000, 600, 200, and 100 LNCaP nuclei in the microscale compared to 100 000 LNCaP nuclei in the macroscale and publicly available LNCaP ChIP-seq ("ENCODE ChIP-Seq"), and C) 3000 nuclei from a patient derived prostate cancer organoid in the microscale.

FRiP scores for all conditions. The macroscale and microscale FRiP scores are plotted showing no significant difference in the slope (Fig. 3D). For inputs above 1000 nuclei (1000–5000), both microscale and macroscale samples had high FRiP scores (mean 41.4% and 36.7%, respectively) (Fig. 3E). However, when we measure FRiP in the low cell number samples, we observed significantly higher FRiP scores using the microscale method compared to the macroscale method (average 30.3% *vs.* 18.2%, $p < 0.0001$) (Fig. 3F). Taken together, this demonstrates that the microscale device allows similar DNA yields and improved signal to noise ratios for peak identification in very low input samples (<1000 nuclei).

We speculate that inputs over 1000 nuclei had a lower yield (Fig. 3A and B) and number of unique reads (Fig. S3C†) using the LAHMAS due to the nuclei being retained in the device. The increased size of the bead and nuclei bolus may result in nuclei and beads shearing off the edge of the bolus that is more distant from the magnet. This phenomenon could be exacerbated in small channels because the channel flattens the bolus and spreads the bead bolus over a larger area. Additionally, a larger bead bolus would be anticipated to transfer a larger carryover volume between wells, which could dilute or alter reagent concentrations. Further optimization of the device for higher input samples including increasing the channel height, magnet strength, and reagent volumes may improve performance for higher cell inputs.

Sequencing quality visualization

FRiP scores give a global indication of sequencing quality but signal intensity at specific genes/promoters and visualization of the patterns of peaks at specific genomic locations is also valuable. *BRN2* (or *POU3F2*) has been proposed to be a driver of prostate cancer differentiation to a neuroendocrine phenotype and therefore has a low mRNA expression in prostate adenocarcinoma models like LNCaPs.[54] Additionally, *BRN2* has been shown to be regulated by Histone H3 lysine 27 trimethylation (H3K27Me3) which leads to closed chromatin and down-regulation of gene expression. For these reasons, we examined detection of H3K27Me3 over the IgG control at the *BRN2* locus in both the microscale and macroscale (Fig. 4A), associated with silencing of this gene's expression in LNCaPs.[44] This contrasts with two genes highly expressed in LNCaPs, *KLK3* and *KLK2*,[54] which, as expected, are devoid of H3K27Me3 peaks (Fig. S4†).

We performed a titration of nuclear inputs in the microscale to assess how decreasing the cell number affects the peaks detected. Our 3000 nuclei input in the microscale performed similarly to our 100 000 nuclei input in the macroscale and favorably to publicly available ChIP-seq (ENCODE Accession #: ENCSR657WLA).[55] With a lower cell input, the peak height decreased but the assays performed in the microscale demonstrated conservation of defined H3K27Me3 peaks from nuclei inputs of 3000 down to 100 (Fig. 4B). Lastly, we were able to assay the epigenetic landscape of nuclei dissociated from patient derived cancer organoids (PDCOs) in the device (Fig. 4C). We observed that yield (LNCaP: 0.147–5.15 [median: 1.13] *vs.* PDO: 5.36), unique reads (LNC: 3 260 613–10 454 899 [median: 6 143 742] *vs.* PDO: 13 098 958), and peaks (LNC: 428–18 697 [median: 737] *vs.* PDO: 92 676) from the PDCO (estimated 1300 cells) were at or above the range observed in the LNCaP sample. The measured MACS2 FRiP (LNCaP: 1.79–29.91 [median: 4.91] *vs.* PDO: 10.21) and peak amplitude at *BRN2* were similar to the averages from 600–2000 nuclei LNCaP inputs on the LAHMAS device (Table S1†) demonstrate the feasibility of assaying primary samples on the LAHMAS device. Taken together, we have demonstrated that CUT&Tag performed on LAHMAS is possible down to 100 nuclei with high FRiP scores and high specificity of detected peaks compared to higher input samples, making the device suitable for use with low input and rare cell sample types.

Conclusions

The OIL-TAS platform provides a number of potential benefits, and here we have focused on its use to develop a complex multistep assay, LAHMAS, to investigate histone modifications from rare cell populations using the CUT&Tag assay. The operation of LAHMAS was optimized for use with small cell inputs and we demonstrated that LAHMAS produces higher sequencing specificity than a macroscale approach for low input samples. We performed CUT&Tag effectively between 100 and 5000 cells on the device with comparable amounts of DNA to the conventional (macroscale) assay, while attaining a higher FriP score on the device for inputs below 1000 cells. The novel pairing of this microfluidic device with a highly sensitive CUT&Tag assay could enable the investigation of chromatin dynamics across a spectrum of rare cell samples. The use of the LAHMAS device could enable epigenetic analysis of samples from patient biopsies or rare cells such as circulating tumor cells to evaluate the contribution of these molecular alterations in tumorigenesis and treatment resistance. The device's compact geometry and standard well pitch may enable future efforts to integrate automation to streamline LAHMAS for clinical research applications. The complexity (both in the number of reaction steps and temperature changes) of the CUT&Tag assay also provides evidence that LAHMAS is capable of performing even very complex multistep assays and thus may find use across a range of potential applications. In any future application requiring consistent device geometry, it would be worthwhile to injection mold the inserts and chambers to reduce batch-to-batch variability inherent to multistep manufacturing procedures.

Data availability

All data needed to evaluate the conclusions in the paper are present in the paper and/or the ESI¶ materials. Our

¶ Electronic supplementary information (ESI) available. See DOI: **https://figshare.com/s/9b1a81f49ed98c0b5a7b**

institutional protocol does not allow unrestricted public access to the raw sequencing data. Therefore, data sharing requests must be submitted to the University of Wisconsin–Madison for review and approval for data related to the patient derived organoid.

Author contributions

Conceptualization: Z. J. K., K. K., D. S. J., M. C. H., D. J. B., J. M. L., and J. M. S. Methodology: Z. J. K., K. K., K. T. H., C. L., M. N. S., E. H., M. C. H., D. J. B., J. M. L., and J. M. S. Device fabrication: Z. J. K., K. K., D. S. J., and C. L. Formal analysis: Z. J. K., K. K., K. T. H., M. N. S., and J. M. S. Investigation: Z. J. K. and K. K. Writing – original draft preparation: Z. J. K., K. K., D. J. B., J. M. L., and J. M. S. Writing – review & editing: Z. J. K., K. K., K. T. H., C. L., M. N. S., E. H., D. S. J., D. F. J., M. C. H., D. J. B., J. M. L., and J. M. S. Visualization: Z. J. K., K. K., and K. T. H. Organoid preparation: E. H. and D. F. J. Supervision: S. G. Z., D. J. B., J. M. L., and J. M. S. Funding acquisition: D. F. J., S. G. Z., M. C. H., D. J. B., and J. M. L.

Conflicts of interest

J. M. L. has consulted with Pfizer on increasing genetic testing for men with prostate cancer. D. J. B. holds equity in Bellbrook Labs LLC, Tasso Inc., Salus Discovery LLC, Lynx Biosciences Inc., Stacks to the Future LLC, Flambeau Diagnostics LLC, and Onexio Biosystems LLC. K. T. H. has a family member who is an employee of Epic Systems. S. G. Z. reports unrelated patents licensed to Veracyte, and has a family member that is an employee of Artera and holds stock in Exact Sciences. K. T. H., S. G. Z., and the University of Wisconsin have filed a provisional patent on previous published fragmentomics work. M. C. H. served as a paid consultant/received honoraria from Pfizer, has received research funding from Merck, Novartis, Genentech, Promicell and Bristol Myers Squibb and has filed patents related to DNA methylation analysis and predictive biomarkers. D. F. J has unrelated patents licensed to Gregour Diagnostics and serves on the SAB. All remaining authors have declared no conflicts of interest.

Acknowledgements

We would like to acknowledge funding from the National Cancer Institute (NCI): P50CA269011 to D. F. J., S. G. Z., D. J. B., and J. M. L., R01CA247479 to M. C. H., D. J. B., and J. M. L., and R50CA293840 to J. M. S.; Department of Defense: W81XWH-21-1-0204 to J. M. L. and M. C. H. W81XWH-21-1-0205 to S. G. Z. and W81XWH-19-1-0164 to J. M. L.; shared research services at the UWCCC Cores are supported by Cancer Center Support Grant [grant number P30 CA014520].

Notes and references

1 S. G. Zhao, J. M. Sperger, J. L. Schehr, R. R. McKay, H. Emamekhoo and A. Singh, *et al.*, A clinical-grade liquid biomarker detects neuroendocrine differentiation in prostate cancer, *J. Clin. Invest.*, 2022, **132**(21), e161858.

2 O. Taryma-Leśniak, K. E. Sokolowska and T. K. Wojdacz, Current status of development of methylation biomarkers for in vitro diagnostic IVD applications, *Clin. Epigenet.*, 2020, **12**, 100.

3 P. Cejas, Y. Xie, A. Font-Tello, K. Lim, S. Syamala and X. Qiu, *et al.*, Subtype heterogeneity and epigenetic convergence in neuroendocrine prostate cancer, *Nat. Commun.*, 2021, **12**(1), 5775.

4 H. S. Kaya-Okur, D. H. Janssens, J. G. Henikoff, K. Ahmad and S. Henikoff, Efficient low-cost chromatin profiling with CUT&Tag, *Nat. Protoc.*, 2020, **15**(10), 3264–3283.

5 P. J. Skene and S. Henikoff, An efficient targeted nuclease strategy for high-resolution mapping of DNA binding sites, *eLife*, 2017, **6**, e21856.

6 B. L. Kidder, G. Hu and K. Zhao, ChIP-Seq: technical considerations for obtaining high-quality data, *Nat. Immunol.*, 2011, **12**(10), 918–922.

7 S. Ma and Y. Zhang, Profiling chromatin regulatory landscape: insights into the development of ChIP-seq and ATAC-seq, *Mol. Biomed.*, 2020, **1**(1), 9.

8 C. Sun and C. Lu, Microfluidics-Based Chromosome Conformation Capture (3C) Technology for Examining Chromatin Organization with a Low Quantity of Cells, *Anal. Chem.*, 2018, **90**(6), 3714–3719.

9 J. D. Buenrostro, B. Wu, U. M. Litzenburger, D. Ruff, M. L. Gonzales and M. P. Snyder, *et al.*, Single-cell chromatin accessibility reveals principles of regulatory variation, *Nature*, 2015, **523**(7561), 486–490.

10 S. Ma, M. de la Fuente Revenga, Z. Sun, C. Sun, T. W. Murphy and H. Xie, *et al.*, Cell-type-specific brain methylomes profiled via ultralow-input microfluidics, *Nat. Biomed. Eng.*, 2018, **2**(3), 183–194.

11 A. Stark, D. J. Shin, T. Pisanic, K. Hsieh and T. H. Wang, A parallelized microfluidic DNA bisulfite conversion module for streamlined methylation analysis, *Biomed. Microdevices*, 2016, **18**(1), 5.

12 Z. Cao, C. Chen, B. He, K. Tan and C. Lu, A microfluidic device for epigenomic profiling using 100 cells, *Nat. Methods*, 2015, **12**(10), 959–962.

13 Z. Liu, L. B. Naler, Y. Zhu, C. Deng, Q. Zhang and B. Zhu, *et al.*, nMOWChIP-seq: low-input genome-wide mapping of non-histone targets, *NAR:Genomics Bioinf.*, 2022, **4**(2), lqac030.

14 S. Ma, Y. P. Hsieh, J. Ma and C. Lu, Low-input and multiplexed microfluidic assay reveals epigenomic variation across cerebellum and prefrontal cortex, *Sci. Adv.*, 2018, **4**(4), eaar8187.

15 T. W. Murphy, Y. P. Hsieh, S. Ma, Y. Zhu and C. Lu, Microfluidic Low-Input Fluidized-Bed Enabled ChIP-seq Device for Automated and Parallel Analysis of Histone Modifications, *Anal. Chem.*, 2018, **90**(12), 7666–7674.

16 M. Adli, J. Zhu and B. E. Bernstein, Genome-wide chromatin maps derived from limited numbers of hematopoietic progenitors, *Nat. Methods*, 2010, **7**(8), 615–618.

17 H. S. Kaya-Okur, S. J. Wu, C. A. Codomo, E. S. Pledger, T. D. Bryson and J. G. Henikoff, *et al.*, CUT&Tag for efficient epigenomic profiling of small samples and single cells, *Nat. Commun.*, 2019, **10**(1), 1930.
18 G. Robertson, M. Hirst, M. Bainbridge, M. Bilenky, Y. Zhao and T. Zeng, *et al.*, Genome-wide profiles of STAT1 DNA association using chromatin immunoprecipitation and massively parallel sequencing, *Nat. Methods*, 2007, **4**(8), 651–657.
19 A. Barski, S. Cuddapah, K. Cui, T. Y. Roh, D. E. Schones and Z. Wang, *et al.*, High-resolution profiling of histone methylations in the human genome, *Cell*, 2007, **129**(4), 823–837.
20 D. S. Johnson, A. Mortazavi, R. M. Myers and B. Wold, Genome-wide mapping of in vivo protein-DNA interactions, *Science*, 2007, **316**(5830), 1497–1502.
21 C. Li, J. Yu, J. Schehr, S. M. Berry, T. A. Leal and J. M. Lang, *et al.*, Exclusive Liquid Repellency: An Open Multi-Liquid-Phase Technology for Rare Cell Culture and Single-Cell Processing, *ACS Appl. Mater. Interfaces*, 2018, **10**(20), 17065–17070.
22 D. S. Juang, T. D. Juang, D. M. Dudley, C. M. Newman, M. A. Accola and W. M. Rehrauer, *et al.*, Oil immersed lossless total analysis system for integrated RNA extraction and detection of SARS-CoV-2, *Nat. Commun.*, 2021, **12**(1), 4317.
23 C. Li, Z. Hite, J. W. Warrick, J. Li, S. H. Geller and V. G. Trantow, *et al.*, Under oil open-channel microfluidics empowered by exclusive liquid repellency, *Sci. Adv.*, 2020, **6**(16), eaay9919.
24 M. Ho, A. Au, R. Flick, T. V. Vuong, A. A. Sklavounos and I. Swyer, *et al.*, Antifouling Properties of Pluronic and Tetronic Surfactants in Digital Microfluidics, *ACS Appl. Mater. Interfaces*, 2023, **15**(5), 6326–6337.
25 C. Li, D. J. Niles, D. S. Juang, J. M. Lang and D. J. Beebe, Automated System for Small-Population Single-Particle Processing Enabled by Exclusive Liquid Repellency, *SLAS Technol.*, 2019, **24**(6), 535–542.
26 Q. Chen, H. Zhai, D. J. Beebe, C. Li and B. Wang, Visualization-enhanced under-oil open microfluidic system for in situ characterization of multi-phase chemical reactions, *Nat. Commun.*, 2024, **15**(1), 1155.
27 C. Li, J. Yu, P. Paine, D. S. Juang, S. M. Berry and D. J. Beebe, Double-exclusive liquid repellency (double-ELR): an enabling technology for rare phenotype analysis, *Lab Chip*, 2018, **18**(18), 2710–2719.
28 Y. Sun, Y. Zheng, C. Liu, Y. Zhang, S. Wen and L. Song, *et al.*, Liquid marbles, floating droplets: preparations, properties, operations and applications, *RSC Adv.*, 2022, **12**(24), 15296–15315.
29 J. Niu, W. Liu, J. X. Li, X. Pang, Y. Liu and C. Zhang, *et al.*, Machining water through laser cutting of nanoparticle-encased water pancakes, *Nat. Commun.*, 2023, **14**(1), 3853.
30 X. Li, X. Pang, H. Jiang, M. Duan, H. Liu and Z. Yang, *et al.*, Open millifluidics based on powder-encased channels, *Proc. Natl. Acad. Sci. U. S. A.*, 2023, **120**(28), e2302907120.
31 H. Liu, X. Pang, M. Duan, Z. Yang, T. P. Russell and X. Li, A Simple Route for Open Fluidic Devices with Particle Walls, *Adv. Mater.*, 2025, **37**(4), e2413862.
32 E. Walsh, A. Feuerborn and P. Cook, *Implementation of a protocol for assembling DNA in a Teflon tube*, SPIE, 2017.
33 S. M. Berry, E. T. Alarid and D. J. Beebe, One-step purification of nucleic acid for gene expression analysis via Immiscible Filtration Assisted by Surface Tension (IFAST), *Lab Chip*, 2011, **11**(10), 1747–1753.
34 B. P. Casavant, D. J. Guckenberger, S. M. Berry, J. T. Tokar, J. M. Lang and D. J. Beebe, The VerIFAST: an integrated method for cell isolation and extracellular/intracellular staining, *Lab Chip*, 2013, **13**(3), 391–396.
35 S. M. Berry, H. M. Pezzi, A. J. LaVanway, D. J. Guckenberger, M. A. Anderson and D. J. Beebe, AirJump: Using Interfaces to Instantly Perform Simultaneous Extractions, *ACS Appl. Mater. Interfaces*, 2016, **8**(24), 15040–15045.
36 B. P. Casavant, D. J. Guckenberger, D. J. Beebe and S. M. Berry, Efficient sample preparation from complex biological samples using a sliding lid for immobilized droplet extractions, *Anal. Chem.*, 2014, **86**(13), 6355–6362.
37 S. M. Berry, L. N. Strotman, J. D. Kueck, E. T. Alarid and D. J. Beebe, Purification of cell subpopulations via immiscible filtration assisted by surface tension (IFAST), *Biomed. Microdevices*, 2011, **13**(6), 1033–1042.
38 S. M. Berry, K. J. Regehr, B. P. Casavant and D. J. Beebe, Automated Operation of Immiscible Filtration Assisted by Surface Tension (IFAST) Arrays for Streamlined Analyte Isolation, *J. Lab. Autom.*, 2013, **18**(3), 206–211.
39 S. M. Berry, H. M. Pezzi, E. D. Williams, J. M. Loeb, D. J. Guckenberger and A. J. Lavanway, *et al.*, Using Exclusion-Based Sample Preparation (ESP) to Reduce Viral Load Assay Cost, *PLoS One*, 2015, **10**(12), e0143631.
40 D. S. Juang, S. M. Berry, C. Li, J. M. Lang and D. J. Beebe, Centrifugation-Assisted Immiscible Fluid Filtration for Dual-Bioanalyte Extraction, *Anal. Chem.*, 2019, **91**(18), 11848–11855.
41 T. S. Rodems, D. S. Juang, C. N. Stahlfeld, C. S. Gilsdorf, T. E. G. Krueger and E. Heninger, *et al.*, SEEMLIS: a flexible semi-automated method for enrichment of methylated DNA from low-input samples, *Clin. Epigenet.*, 2022, **14**(1), 37.
42 M. Bartosovic, M. Kabbe and G. Castelo-Branco, Single-cell CUT&Tag profiles histone modifications and transcription factors in complex tissues, *Nat. Biotechnol.*, 2021, **39**, 825–835.
43 D. H. Janssens, M. P. Meers, S. J. Wu, E. Babaeva, S. Meshinchi and J. F. Sarthy, *et al.*, Automated CUT&Tag profiling of chromatin heterogeneity in mixed-lineage leukemia, *Nat. Genet.*, 2021, **53**(11), 1586–1596.
44 V. B. Venkadakrishnan, A. G. Presser, R. Singh, M. A. Booker, N. A. Traphagen and K. Weng, *et al.*, Lineage-specific canonical and non-canonical activity of EZH2 in advanced prostate cancer subtypes, *Nat. Commun.*, 2024, **15**(1), 6779.
45 S. Henikoff, J. G. Henikoff, H. S. Kaya-Okur and K. Ahmad, Efficient chromatin accessibility mapping in situ by nucleosome-tethered tagmentation, *eLife*, 2020, **9**, e63274.

46 E. Heninger, D. Kosoff, T. S. Rodems, N. Sethakorn, A. Singh and H. Gungurthi, *et al.*, Live cell molecular analysis of primary prostate cancer organoids identifies persistent androgen receptor signaling, *Med. Oncol.*, 2021, **38**(11), 135.

47 H. Li and R. Durbin, Fast and accurate long-read alignment with Burrows-Wheeler transform, *Bioinformatics*, 2010, **26**(5), 589–595.

48 Y. Zhang, Y. H. Lin, T. D. Johnson, L. S. Rozek and M. A. Sartor, PePr: a peak-calling prioritization pipeline to identify consistent or differential peaks from replicated ChIP-Seq data, *Bioinformatics*, 2014, **30**(18), 2568–2575.

49 S. G. Landt, G. K. Marinov, A. Kundaje, P. Kheradpour, F. Pauli and S. Batzoglou, *et al.*, ChIP-seq guidelines and practices of the ENCODE and modENCODE consortia, *Genome Res.*, 2012, **22**(9), 1813–1831.

50 Y. Zhang, T. Liu, C. A. Meyer, J. Eeckhoute, D. S. Johnson and B. E. Bernstein, *et al.*, Model-based analysis of ChIP-Seq (MACS), *Genome Biol.*, 2008, **9**(9), R137.

51 J. M. Gaspar, Improved peak-calling with MACS2, *bioRxiv*, 2018, preprint, DOI: **10.1101/496521**.

52 Ohnesorge Number, in *Encyclopedia of Microfluidics and Nanofluidics*, ed. D. Li, Springer US, Boston, MA, 2008, p. 1513.

53 L. Shu, T. O. Khor, J. H. Lee, S. S. Boyanapalli, Y. Huang and T. Y. Wu, *et al.*, Epigenetic CpG demethylation of the promoter and reactivation of the expression of Neurog1 by curcumin in prostate LNCaP cells, *AAPS J.*, 2011, **13**(4), 606–614.

54 J. L. Bishop, D. Thaper, S. Vahid, A. Davies, K. Ketola and H. Kuruma, *et al.*, The Master Neural Transcription Factor BRN2 Is an Androgen Receptor-Suppressed Driver of Neuroendocrine Differentiation in Prostate Cancer, *Cancer Discovery*, 2017, **7**(1), 54–71.

55 Y. Luo, B. C. Hitz, I. Gabdank, J. A. Hilton, M. S. Kagda and B. Lam, *et al.*, New developments on the Encyclopedia of DNA Elements (ENCODE) data portal, *Nucleic Acids Res.*, 2020, **48**(D1), D882–D889.

